Polymer 65 (2015) 134–142

Contents lists available at ScienceDirect

Polymer

journal homepage: www.elsevier.com/locate/polymer

Synthesis, characterization and properties of poly(propylene-1-octene)/graphite nanosheet nanocomposites obtained by *in situ* polymerization

Marcéo A. Milani [a], Darío González [b], Raúl Quijada [b], Rosario Benavente [c], Javier Arranz-Andrés [c], Griselda B. Galland [a, *]

[a] Instituto de Química, Universidade Federal do Rio Grande do Sul, Av. Bento Gonçalves 9500, 91501-970 Porto Alegre, Brazil
[b] Departamento de Ingeniería Química, Facultad de Ciencias Físicas y Matemáticas, Universidad de Chile, Casilla 2777 y CIMAT, Santiago, Chile
[c] Instituto de Ciencia y Tecnología de Polímeros, ICTP-CSIC. Juan de la Cierva, 3, 28006 Madrid, Spain

ARTICLE INFO

Article history:
Received 4 February 2015
Received in revised form
23 March 2015
Accepted 24 March 2015
Available online 31 March 2015

Keywords:
Graphite nanosheets
In situ polymerization
Poly(propylene-1-octene)

ABSTRACT

Poly(propylene-1-octene)/graphite nanosheet (PPC8/GNS) nanocomposites with different comonomer and graphite nanosheet (GNS) contents were synthesized by *in situ* polymerization using metallocene catalyst. There was a significant increase in the crystallization temperature of all the nanocomposites. Isothermal crystallization studies by optical microscopy confirmed that the GNSs act as nucleating agent increasing the crystallization rate in the nanocomposites. Transmission electron micrographs showed a good dispersion of the nanoparticles. Mechanical properties confirm the reinforcing effect that the nanoparticles confer to the polymer, especially increasing the modulus. Impedance measurements proved that the conductivity of the nanocomposites increase up to 11 orders of magnitude compared to neat polymers. The main novelty of this work is the control of the nanocomposite properties through the variation of the comonomer and the graphite nanosheets contents.

1. Introduction

The demand for materials containing graphite has been significantly increasing in recent years. Even more interesting is the use of graphene or graphite nanosheets (GNS or GNP), which have outstanding mechanical, electrical and barrier properties and are some of the most promising materials of the future [1,2]. The introduction of these particles into polymeric matrixes for the preparation of micro- or nanocomposites has shown great potential due to the improvements that these fillers are able to provide in the polymers [3–5].

An important feature that some studies with graphite or its derivatives and polyolefins have been reported is the increase in the crystallization temperature (T_c), which decreases the number of processing cycles [6]. In our recent work using *in situ* polymerization to obtain polyethylene/GNS nanocomposites, the crystallization temperature did not show a clear trend [7]; however, polypropylene/GNS nanocomposites had an increase in the T_c up to 10 °C depending on the amount of GNSs added to the reactor [8,9]. However, fillers normally produce polymers that exhibit low elongation and become more brittle in the presence of the nanoparticles. Depending on the matrix used, it may be interesting to prepare composites of copolymers, which are generally more flexible [10,11]. The preparation of nanocomposites with graphite or its derivatives and polyolefin copolymers by mixing the components in an extruder or in solution has been reported by some authors [12–16]. However, only a few works have used *in situ* polymerization to prepare nanocomposite copolymers with graphite or its derivatives, which can have an even better ability to disperse the nanofillers in the polymer matrix [17,18]. Most of these studies are related to polystyrene (PS) copolymers [19–21].

Recently, we were among the first groups to report the synthesis and full characterization of nanocomposites of polypropylene homopolymers with graphite nanosheets (GNS) by *in situ* polymerization using metallocene catalysts [8,9]. These studies showed a remarkable strengthening effect of the matrix with the incorporation of GNS through significant increase in Young's and storage modules, but the stiffness that the graphite nanosheets provided to the polypropylene matrix made those polymers too brittle. Thus, in this work we chose to synthesize PP copolymers, which should be

* Corresponding author. Tel.: +55 5133087317; fax: +55 5133087304.
E-mail address: griselda.barrera@ufrgs.br (G.B. Galland).

http://dx.doi.org/10.1016/j.polymer.2015.03.069
0032-3861/

more flexible than the homopolymer, even in the presence of a nanofiller, being the first study to synthesize nanocomposites of polyolefin copolymers with GNS by *in situ* polymerization. The purpose was also to study how the filler influences the catalytic activity of the system and the resulting polymer properties such as crystallization, degradation temperature, mechanical reinforcement and conductivity.

2. Experimental

2.1. Materials

Expanded graphite (Micrograf HC11) with platelet diameter of around 50 μm was provided by Nacional de Grafite Ltda. (Brazil) [22]. X-Ray diffraction, the transmission and scanning electron microcopies and the atomic force microscopy of the filler has been published in reference 7. GNS has a crystal size of 28 nm [7]. CHN showed an amount of C: 97.5% and O: 2.4%. Raman spectra is provided in the supplementary data.

Toluene and 1-octene were distilled with metallic sodium and benzophenone. Methylaluminoxane -MAO- (Chemtura, 5 wt.% Al solution in toluene) and the metallocene catalyst *rac*-$Me_2Si(Ind)_2ZrCl_2$ (Chemtura) were used as received.

2.2. Preparation of the graphite nanosheets (GNS)

The expanded graphite was suspended in 70% ethanol, and the suspension was treated with an ultrasound bath for 8 h. Then, the suspension was filtered, and the graphite nanosheets were dried at 120 °C for a period of 48 h [7].

2.3. Polymerization reactions

The polymerization reactions were performed at a controlled temperature (40 °C) using a 1000 mL Büchi glass reactor equipped with mechanical stirring. First, toluene as the solvent, MAO (Al/Zr = 1000) as the cocatalyst and 1-octene as the comonomer were added to the reactor. Afterwards, the reactor was fed with propylene, and the catalyst *rac*-$Me_2Si(Ind)_2ZrCl_2$ (5×10^{-6} mol) was added. The reactor was continuously fed with propylene to maintain a constant pressure of 2.8 bar during 0.5 h. In the polymerizations to obtain nanocomposites, graphite nanosheets were added to the reactor using variable amounts. The polymerizations were terminated by the addition of a 10 vol.% HCl in ethanol solution. The polymers were washed with water and dried until they maintained a constant weight.

2.4. Characterizations of polymers

The molecular weights were estimated using a Waters Alliance GPC 2000 instrument equipped with three Styragel HT-type columns (HT3, HT5, and HT6E). 1,2,4-Trichlorobenzene was used as the solvent with a flow rate of 1 mL min^{-1} and temperature of 135 °C. The polymeric microstructure was determined by ^{13}C NMR. The spectra were attained at 130 °C in a Varian Inova 300 operating at 75 MHz. Sample solutions of the polymers were prepared in *o*-dichlorobenzene and benzene-d_6 (20% v/v) in 5 mm sample tubes. The tacticity and percentage of incorporation of the comonomers were determined from the spectra [23,24]. Transmission electronic microscopy (TEM) images were achieved using a JEOL 1200 ExII transmission electron microscope operated at 100 kV. Samples were prepared from ultrathin films (~70 nm) cut under cryogenic conditions with a Leica Ultracut UCT microtome at −80 °C and placed on a copper grid of 300 meshes covered with amorphous carbon. For monitoring the crystallization, an optical microscope (Leica DMLM) was used with a coupled temperature-controlled stage (Linkam LTS350). The samples were placed between glass slides, melted above the melting point, quenched to the desired isothermal crystallization temperature, and examined under crossed polarizers to view the structure evolution. Film samples of polymers (around 350 μm) were obtained from the reactor powder by compression molding in a Collin press between hot plates (about 30 °C above T_m) at a pressure of 20 bar for 5 min. A fast quench (rate around 80 °C/min) between plates refrigerated with cold water was applied after melting in the press. Calorimetric analyses were carried out in a TA Instruments Q100 calorimeter calibrated with different standards, operating at a heating rate of 20 °C min^{-1} and in a temperature range from 25 to 160 °C. The melting temperature, T_m, was determined in the second scan, and the degree of crystallinity was calculated from the enthalpy of fusion data obtained from the DSC curves (162 J g^{-1} was used for a 100% crystalline material [25]). For nanocomposites analysis the mass content of graphite was discounted. Thermogravimetric analysis (TGA) was performed on an SDT Q600 thermal analyzer Q20 (TA Instruments) at a scanning rate of 20 °C min^{-1} within a temperature range from 25 to 1000 °C. The tensile properties were evaluated in an Instron model 3366 dynamometer with a 100 N load cell. Dumbbell-shaped samples with an effective thickness of 0.3 mm, a gauge length of 15 mm and a width of 2 mm were cut from those compression-molded sheets. The samples were tested at a rate of 10 mm min^{-1} at room temperature. Each set of measurements was repeated five times. Viscoelastic properties were measured in a Polymer Laboratories MK II dynamic mechanical thermal analyzer working in a tensile mode. The complex modulus and the loss tangent for each sample were determined at 1, 3, 10 and 30 Hz over a temperature range from −140 to 150 °C, at a heating rate of 1.5 °C/min. A Vickers indentor attached to a Leitz microhardness (MH) tester was used to carry out microindentation measurements. Experiments were undertaken at 25 °C. A contact load of 0.98 N and a contact time of 25 s were employed. MH values (in MPa) were calculated according to the relationship: $MH = 2 \sin 68° \, P/d^2$, where P (in N) is the contact load and d (in mm) is the diagonal length of the projected indentation area. Electrical conductivity of the nanocomposites was obtained by impedance measurements. The experiments were performed Novocontrol broadband dielectric spectrometer (Hundsagen, Germany) integrated by a SR 830 lock-in amplifier with an Alpha dielectric interface in the frequency range $10^{-2} - 10^7$ Hz The electrodes used were gold disks of 10 mm of diameter. The temperature was controlled by a nitrogen jet (QUATRO from Novocontrol) with a temperature error of 0.1 K during every single sweep in frequency. Thus, the electrical conductivity of the polymeric film could be calculated by the following equation: $\sigma = 1/Rb \, (d/S)$. Where σ is the electrical conductivity, d is the film thickness, S is the area of electrodes contacting the polymeric film and Rb the bulk resistance.

3. Results and discussion

3.1. Synthesis of the PPC8 matrix

1-Octene comonomer was chosen to be inserted in the polypropylene chain with the aim of obtaining a polymer with long branches that would decrease the crystalline organization of the chains. As the final objective of the copolymerization was to obtain a more flexible polypropylene than the PP homopolymer, but with good mechanical properties, we used small amounts of 1-octene because the comonomer normally decreases the molecular weights and the Young's modulus of the polymers.

Three copolymers with different amounts of comonomers were synthesized and characterized by GPC, ^{13}C NMR and DSC (Table 1).

Table 1
Synthesis and characterization of the PPC8 matrix.

Entry	1-C_8 added (mol/L)	Activity (KgPP/bar h molZr)	M_w (g/mol)	M_w/M_n	Tacticity m (mol%)	1-C_8 incorporated (mol%)	T_c (°C)	T_m (°C)	X_c (%)
1	–	14,643	70,200	1.4	96.7	–	108	143	62
2	0.127	14,229	62,100	1.5	94.9	1.5	88	128	45
3	0.159	14,157	60,100	1.4	96.3	2.4	83	124	40
4	0.191	13,971	57,000	1.6	94.4	2.9	81	123	38

The addition of 1-octene caused a decrease of the molecular weights compared with the homopolymer. However, this variation is not enough significant, that could limit the studies related with the macrostructure. Those molecular weights are in the limit, below which mechanical properties become dependent of them. On the other hand, the polydispersity showed no changes.

^{13}C NMR analysis showed that the addition of a second comonomer did not affect the stereoregularity of the matrix because the changes in tacticity are within the experimental error of this technique.

Finally, the DSC analysis confirmed the synthesis of the PPC8 matrix due to differences in the crystal structure caused by the insertion of 1-octene. By acting as imperfections, the comonomers provide the formation of smaller crystals that are slower to crystallize, therefore decreasing the crystallization temperature (T_c). These smaller crystals melt at lower temperatures, which also decrease the melting temperature (T_m). The results in Table 1 show that when the comonomer content was increased, lower values of T_c, T_m and the degree of crystallinity (X_c) were observed.

3.2. Synthesis and thermal properties of the PPC8/GNS nanocomposites

Once the amounts of 1-octene to be inserted in the PP matrix were chosen, the polymerization reactions for the synthesis of nanocomposites by *in situ* polymerization were performed at the same experimental conditions. In this step, variable amounts of the GNSs were added to the reactor for each amount of 1-octene. Table 2 shows the results of the synthesis and properties of the nanocomposites with variable amounts of graphite nanosheets PPC8 (PPC8-X, X = amount of 1-octene in mol%).

The GNS contents calculated from the reaction yields or through the residues in the TGA curves exhibit very similar values, indicating homogeneity of the samples. Throughout the text, the percentage of GNSs referred to is the value obtained using TGA. The reported activities, in Table 2, were calculated by subtracting the amount of added GNS in each case.

The catalytic activity tends to decrease with an increase in the GNS content, most likely due to the presence of polar groups on the surface of graphene, which can deactivate the metallocene catalyst. The DSC results showed that the increase in the amount of GNSs did not produce significant changes in the values of the melting temperature (T_m) and the degree of crystallinity (X_c). On the other hand, an increase in the crystallization temperature (T_c) was observed. The thermal properties showed exactly the same behavior in all the copolymers with different amounts of comonomer. All of the nanocomposites showed an increase in the crystallization temperature (T_c) of around 10 °C for approximately 16–18% of GNS. This pronounced effect shows the nucleation power of graphite nanosheets. Fig. 1a, shows the significant

Table 2
Synthesis and properties of the PPC8/GNS nanocomposites.

Samples	GNS[a] (%)	GNS_{TGA}[b] (%)	Activity[c]	T_c (°C)	T_m (°C)	X_c (%)	T_{onset} (°C)	T_{max} (°C)	E[d] (MPa)	σ_Y[e] (MPa)	σ[f] (MPa)	ε[g] (%)	MH[h] (MPa)	T_g[i] (°C)	T_α[j] (°C)
PPC8-1.5	–	–	19,950	88	128	45	431	460	738 ± 19	19.8 ± 1.8	19.8 ± 1.8	322 ± 44	55.4 ± 1.6	7.5	51.8
PPC8-1.5	1.5	1.6	16,250	90	126	46	435	462	801 ± 17	20.5 ± 1.4	20.5 ± 1.4	234 ± 31	55.8 ± 1.0	12.2	51.8
PPC8-1.5	3.1	2.9	13,030	91	127	43	444	467	823 ± 18	20.3 ± 1.6	20.3 ± 1.6	109 ± 15	57.9 ± 2.1	–	–
PPC8-1.5	4.6	4.4	12,570	93	126	44	443	468	832 ± 36	21.1 ± 0.3	21.1 ± 0.3	42 ± 8	57.8 ± 2.8	12.1	54.0
PPC8-1.5	9.8	10.7	8460	95	128	45	452	476	968 ± 44	–	18.1 ± 1.5	5.5 ± 0.9	59.7 ± 3.8	12.0	55.4
PPC8-1.5	12.0	11.9	8160	95	128	39	459	479	1094 ± 67	–	19.5 ± 2.4	4.7 ± 1.1	60.8 ± 1.9	–	–
PPC8-1.5	18.7	18.8	6170	97	127	42	460	479	1113 ± 18	–	22.3 ± 2.7	3.8 ± 1.6	70.9 ± 2.5	–	–
PPC8-2.4	–	–	18,410	83	124	40	426	458	658 ± 57	18.9 ± 0.7	18.9 ± 0.7	515 ± 44	45.6 ± 2.7	5.8	51.5
PPC8-2.4	1.1	1.0	14,070	86	125	40	433	462	733 ± 21	19.9 ± 0.8	19.9 ± 0.8	491 ± 33	48.1 ± 1.7	5.7	51.1
PPC8-2.4	3.0	3.4	13,310	87	124	42	440	466	739 ± 43	21.5 ± 1.3	21.5 ± 1.3	95 ± 5	48.1 ± 0.8	–	–
PPC8-2.4	5.0	4.7	12,120	88	123	44	443	467	773 ± 33	22.6 ± 1.2	22.6 ± 1.2	59 ± 4	51.7 ± 1.9	6.6	52.4
PPC8-2.4	11.2	11.2	6910	88	123	40	445	472	889 ± 41	–	18.6 ± 0.5	8.6 ± 0.1	54.1 ± 4.7	7.3	52.8
PPC8-2.4	12.9	12.8	5440	88	123	38	452	473	947 ± 24	–	19.2 ± 0.5	7.1 ± 0.2	53.1 ± 0.7	–	–
PPC8-2.4	16.4	17.3	3140	93	124	40	457	475	1034 ± 74	–	19.2 ± 1.0	4.3 ± 1.7	56.9 ± 1.8	–	–
PPC8-2.9	–	–	17,640	81	123	38	425	457	532 ± 41	17.9 ± 1.4	23.3 ± 3.5	732 ± 50	41.7 ± 1.0	5.3	51.2
PPC8-2.9	1.4	1.4	13,310	83	124	36	432	461	571 ± 11	19.7 ± 1.3	24.5 ± 2.5	620 ± 29	43.7 ± 2.8	6.5	52.1
PPC8-2.9	4.9	4.4	8240	87	123	38	441	469	710 ± 33	21.1 ± 2.9	21.1 ± 3.0	400 ± 45	47.6 ± 1.4	–	–
PPC8-2.9	8.3	8.9	7920	87	122	37	442	468	738 ± 37	21.1 ± 0.6	21.3 ± 0.6	32 ± 2	46.3 ± 0.9	5.7	51.4
PPC8-2.9	10.1	10.7	7370	89	122	38	448	475	811 ± 49	–	18.9 ± 1.4	6.1 ± 0.5	48.3 ± 2.1	5.8	52.3
PPC8-2.9	12.6	12.6	6140	90	123	35	454	477	894 ± 44	–	24.5 ± 2.8	6.4 ± 0.8	49.0 ± 0.7	–	–
PPC8-2.9	17.2	17.5	3980	91	121	38	456	476	1002 ± 26	–	24.9 ± 1.6	6.5 ± 1.8	51.2 ± 3.7	–	–

Reactions conditions: P = 2.8 bar, T = 40 °C, [Zr] = 5 μmol, Al/Zr = 1000, t = 30 min. V_{tol} = 500 mL.
[a] GNS percentage calculated from the reaction yield.
[b] GNS percentage obtained from the TGA residue.
[c] Catalytic activity of the polymerization reaction = (kg PP/n_{Zr} bar h).
[d] Young's Modulus.
[e] Yield stress.
[f] Tensile strength.
[g] Elongation.
[h] Microhardness.
[i] Glass transition temperature obtained by DMTA analysis.
[j] α relaxation temperature obtained by DMTA analysis.

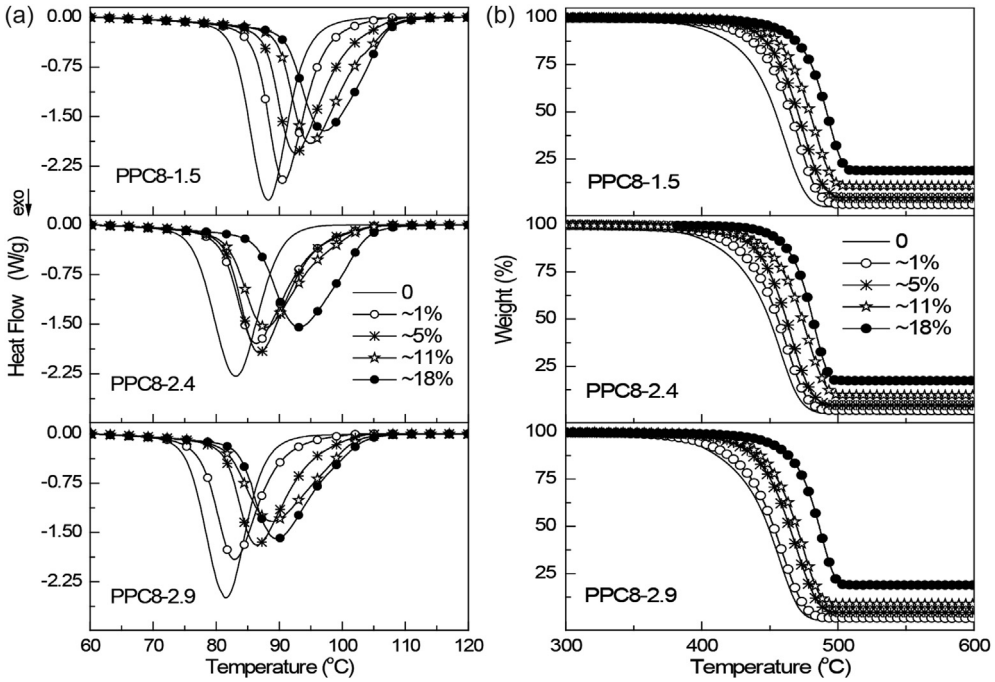

Fig. 1. Curves for PPC8 copolymers and their PPC8/GNS nanocomposites: a) DSC -crystallization process; b) TGA.

displacement of T_c for each PPC8 matrix used. Although the crystallinity it is not significantly altered, the curves become increasingly broader as the amount of GNSs is increased. This result is due to the presence of different nucleation points that are formed, which increases the range of crystallization. The thermogravimetric analysis, in addition to providing the GNS content, also allowed us to observe the improvement in thermal stability that the nanoparticles provided to the copolymers (Fig. 1b). In fact, the increase in the GNS content in the nanocomposites led to an increase in both the initial degradation temperature (T_{onset}) and the maximum weight loss temperature (T_{max}), up to approximately 30 °C and 20 °C, respectively, for approximately 16–18% of GNS.

3.3. Mechanical properties

Table 2 also shows the results obtained for the mechanical properties of the PPC8 nanocomposites with graphite nanosheets. The increased in the amount of GNS provided a significant change in stiffness of the synthesized nanocomposites. PPC8-1.5 and PPC8-2.4 copolymers nanocomposites showed a very similar behavior, that is, an increase of 50% in the elastic modulus for the highest GNS content and a change from ductile to brittle fracture for values above 4.4 (entry 7) and 4.7% (entry 13) of GNS, respectively. On the other hand, the PPC8-2.9 samples had an increase in the elasticity modulus at the highest filler content (entry 22) of around 100% and are still ductile with 4.4% of GNS (entry 18) and the change of fracture behavior only occurred above 8.9% of GNS (entry 19). After this change at the fracture, nanocomposites fail to present a plastic region; they have instead a sharp drop in elongation. It is noticed that while the nanocomposites exhibit a plastic behavior, the increase of the GNS percentages provides greater yield stress. In Fig. 2a one can observe the comparison between nanocomposites with different matrices. The homopolymer iPP/GNS 4.4% had an elongation of 2.5% [9], while the copolymer PPC8-2.9–4.4% (entry 18) with the same GNS content shows 400%. Even the copolymer PPC8-2.9 with a GNS content of 8.9% (entry 19) has an elongation of 32% which is superior to that of the homopolymer with 4.4% of GNS. Fig. 2b shows the tensile test detail for the PPC8-2.9 copolymer and their nanocomposites. Values found in tensile strength are more complexes. The PPC8-1.5 and PPC8-2.4 copolymers showed a

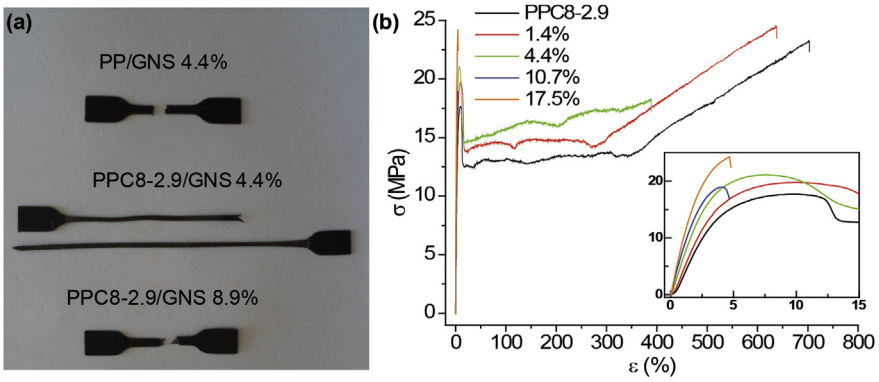

Fig. 2. Images of specimens after tensile tests (a) and curves obtained in the tensile tests of the PPC8-2.9 and their nanocomposites (b).

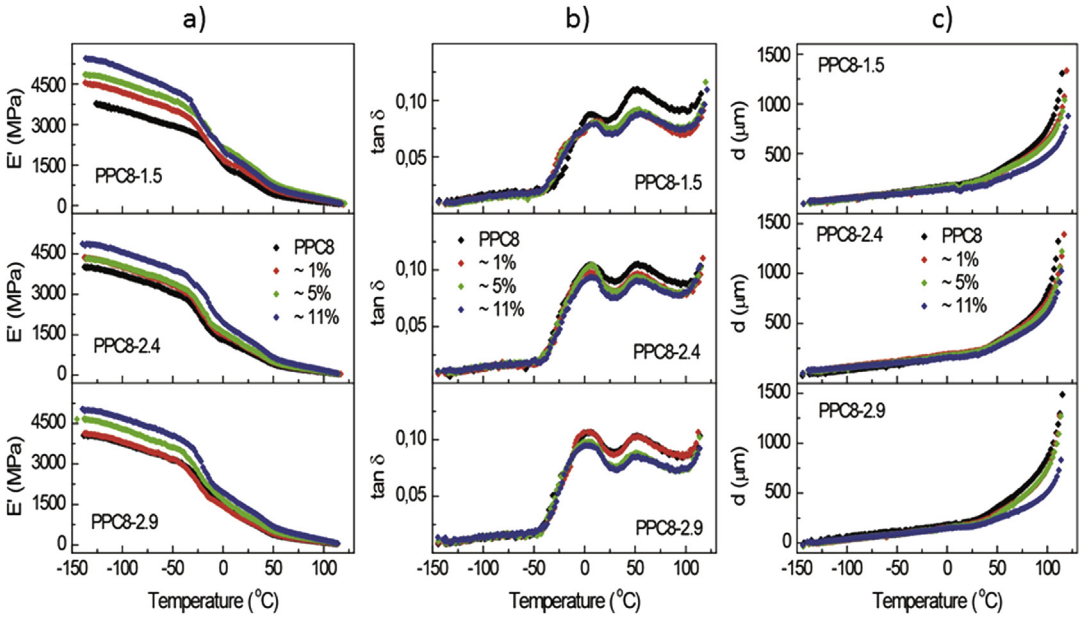

Fig. 3. DMA results of PPC8 and their nanocomposites: storage modulus (a), tan δ (b) and dimensional stability (c).

maximum tensile strength in the flow region before breaking. On the other hand PPC8-2.9, being more ductile, showed the maximum tensile strength at break for 0–1.4% of GNS (entries 4 and 17), indicating the strain hardening process. However, as the amount of GNS increases the elongation decreases and at 4.4–8.9% of GNS (entries 18 and 19) the maximum tensile strength value is also equal to the yield stress value. It is noteworthy that all the copolymers clearly exhibited a tendency to increase the tensile strength with the amount of GNS, either in the plastic zone (moderate and high elongation) or in the elastic area (small elongation).

The viscoelastic behavior of the system was studied by DMA analysis. The change in storage modulus with temperature for some PPC8/GNS nanocomposites can be seen in Fig. 3a. The strengthening effect provided by the GNS, observed by the increase of the Young's modulus is also noted here, since the addition of GNS increased significantly the storage modulus of the nanocomposites. It is clearly shown that, over the entire temperature range of the experiment, the nanocomposites showed higher stiffness than the neat polymer. The results visualized and extracted from the tan δ graphs (Fig. 3b) confirm what it was mentioned above. Due to the increase difficulty in mobility imposed by the addition of the filler, the relaxation processes α and β have lower intensities for the nanocomposites. Furthermore, through the β relaxation it can be seen that the glass transition temperatures were slightly increased (in tan δ at 3 Hz), as well as the temperatures related to movements within the crystals (α) (Table 2). In relation to the deformability, the increase in the amount of filler also resulted in an increase in the dimensional stability of the matrix. In Fig. 3c, it can be seen that above T_g the nanocomposites need a higher temperature to have the same deformation than the neat copolymer.

The variation of microhardness with GNS amounts is also detailed in Table 2. It can be seen that the stiffness of the graphite nanosheets increased significantly the microhardness of the nanocomposites, exhibiting the same behavior observed for the Young's modulus. The microhardness (MH) is defined as the local resistance of a material to undergo a permanent deformation after the application of a force. The deformation of a polymer under the action of the penetrator, is basically governed by the viscoelastic and plastic components, which also regulate the mechanical properties of the material [26]. Thus, there is normally a direct relationship between the mechanical properties and microhardness [27,28]. Fig. 4 shows the relationship of the microhardness, Young's modulus and storage modulus (at 25 °C and 3 Hz) with increasing of GNS content for copolymers and their nanocomposites. It is clearly shown that the increased stiffness provided

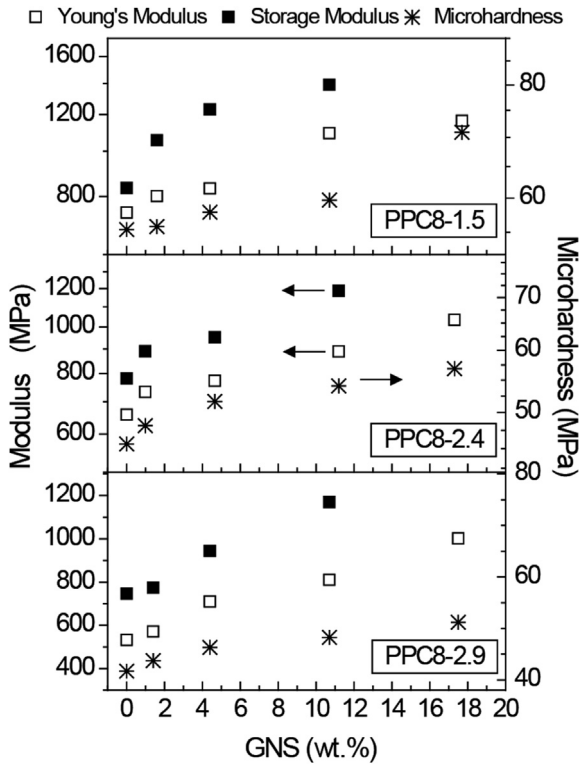

Fig. 4. Relationship of microhardness (MH) with Young (○) and storage (●) modules for polymers with different levels of GNS.

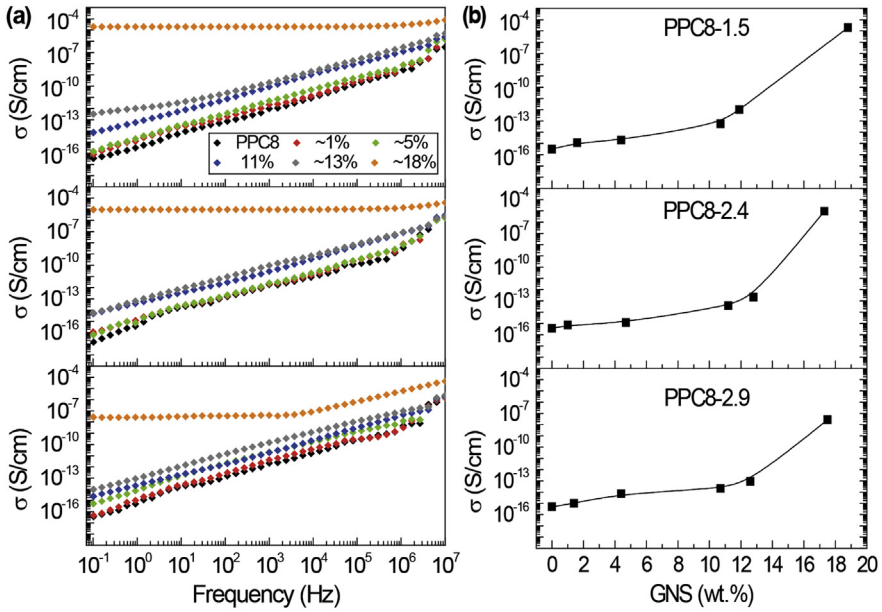

Fig. 5. Conductivity of PPC8 and PPC8/GNS nanocomposites in function of frequency.

by graphite nanosheets leads to a continuous increase in microhardness values. Moreover, one can also notice this nearly linear relationship of the microhardness with the Young and storage modules.

3.4. Electrical conductivity

Fig. 5a shows the graphs obtained for the conductivity values through a scan at several frequencies. At high frequencies, almost all materials are able to present certain conductivity, however, since this is an unusual condition, are considered conductors and semiconductors those materials with high values of conductivity even at low frequencies [29].

The electrical conductivity of the copolymers and nanocomposites with filler contents up to approximately 5 wt.-% is practically null at low frequencies. When this content increases till 10–13 wt;-%, although the conductivity remain virtually nonexistent, one can observe a small change in the curves, especially for the nanocomposites with lower 1-octene content. The nanocomposites only approximated to a semiconductor behavior when the GNS percentage added was about 17–18 wt.-%, where a very significant change occurred in the curves. It can be noticed that at these percentages the variation of conductivity with the frequency is quite low, a typical behavior of ideal conductive or semiconductor material. To better visualize the role of graphite nanosheets in different nanocomposites, graphs (Fig. 5b) of conductivity values at the frequency of 1 Hz of the PPC8-X and PPC8-X/GNS nanocomposites were plotted. The profiles of the curves makes clear that increasing the GNS content of the nanocomposites, a steady increase in conductivity occurs reaching the percolation and transforming the nanocomposites in semiconductors. Taking into account the maximum conductivity values, the increase for PPC8-1.5/GNS, PPC8-2.4/GNS and PPC8-2.9/GNS nanocomposites was 10^{11}, 10^{10} and 10^{7} times, respectively. PPC8-1.5/GNS nanocomposites showed a percolation threshold between 12 and 14% of GNS, while the estimated value for the PPC8-2.4/GNS and PPC8-2.9/GNS is around 13 and 15%. It seems that the higher amount of amorphous phase in the nanocomposite copolymers and higher heterogeneity of the crystals could hamper the graphite nanosheets pre-contact (conductive network formation), thus impairing the conductivity.

3.5. TEM of the nanocomposites

Fig. 6 presents the transmission electron micrographs obtained for the PPC8-1.5_1.6% nanocomposite (entry 5, Table 2). In Fig. 6a,

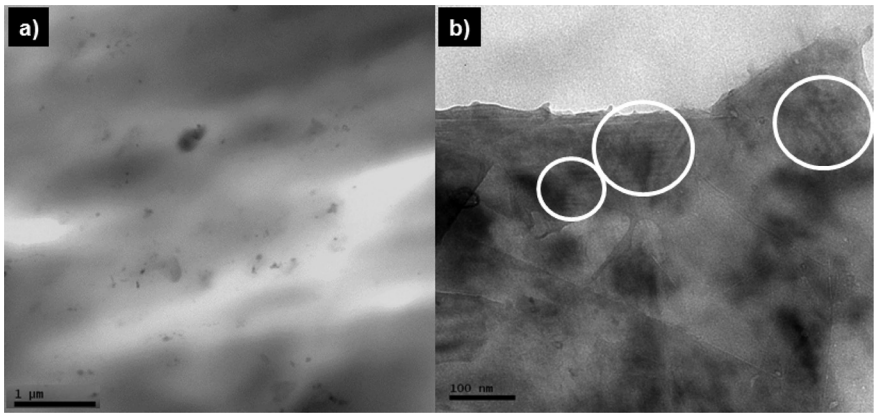

Fig. 6. Transmission electron micrographs of the PPC8-1.5_1.6% nanocomposite at different scales (1 μm and 100 nm).

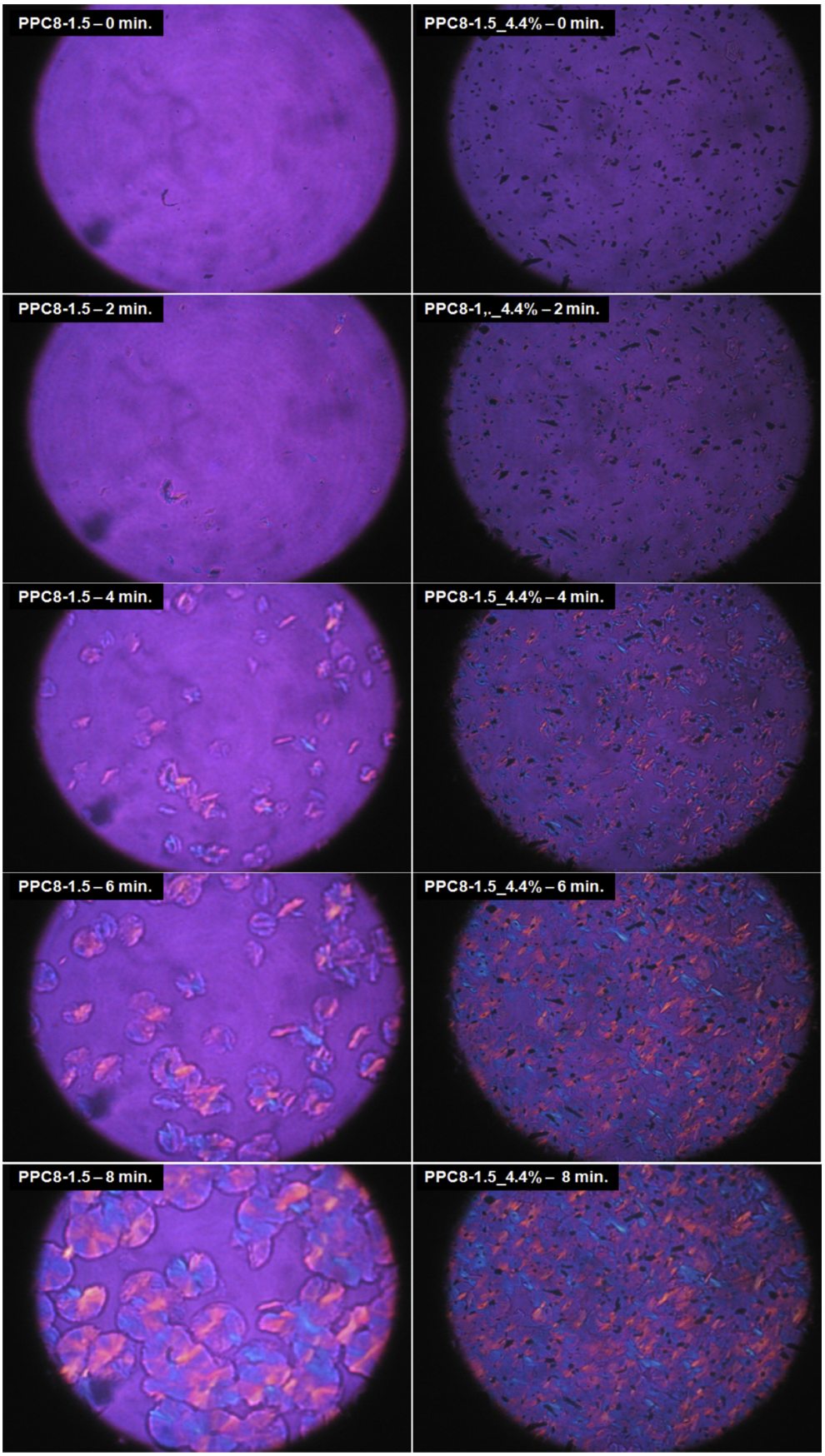

Fig. 7. Images obtained using optical microscopy of PPC8-1.5 and PPC8-1.5_4.4% during isothermal crystallization (total width of the photograph frame is 216 μm).

the graphite nanosheets are well distributed in the polymeric matrix of the nanocomposite along the area analyzed. Fig. 6b shows a higher magnification image of the extremities of the sample to more easily illustrate the nanosheets in the nanocomposite.

3.6. Optical microscopy during isothermal crystallization

The crystallization behavior versus time was investigated using optical microscopy of the PPC8 neat copolymer and the PPC8/GNS-1.5_4.4% nanocomposite (entry 7, Table 2). The methodology employed was isothermal crystallization, which consists of submitting the polymers to a constant temperature at which they are able to crystallize, i.e., a temperature between T_c and T_m. Thus, the polymers were left at 112 °C, and micrographs were obtained every 2 min, as shown in Fig. 7.

At t = 0, the polymers were completely melted, being possible to observe only a few agglomerates of GNSs in the nanocomposite. After 2 min, the first nucleation centers for both copolymers were formed, having the nanocomposite a greater number of them. At t = 4 min, additional nucleation sites appeared for PPC8, while the nanocomposite had crystallized in all directions. It is noteworthy that the crystals in the nanocomposite did not grow only around the visible agglomerates but also at various points, indicating that much smaller nucleating centers exist. After 6 min, no more new nuclei arose, but it seemed that the crystals formed in the first 4 min began to grow in all directions. At 8 min, the nanocomposite no longer had many spaces for the growth of the crystals, so they began to grow on top of each other, while the PPC8 spherulites still had considerable space to grow. In the nanocomposite, the nucleation sites provided the formation of smaller crystals, and only a few spherulites were observed.

This study illustrates that graphite nanosheets act as nucleating agents for polymers, facilitating the formation of crystals. This decrease in crystallization time is much sought in the industry, as it directly corresponds to shorter processing times.

4. Conclusions

PPC8 nanocomposites with graphite nanosheet (GNS) contents between 1.6 and 18.8 wt.% were obtained by *in situ* polymerization. The crystallization studies showed that the nanoparticles act as nucleating agents in the polymer, significantly increasing the crystallization temperature (approximately 10 °C) which permit to decrease the processing times. In addition, the nanocomposites also showed an improvement in thermal stability with an increase of more than 20 °C in the degradation temperatures. The graphite nanosheets increased significantly the Young's modulus of the PPC8 copolymers, and this increase in stiffness is responsible for the reduction of elongation. Moreover, the copolymer containing 2.9% of 1-octene and 4.4% of GNS has a very good elongation (400%) when the homopolymer with the same amount of graphite was very brittle (2.5% of elongation). The reinforcing effect caused by the incorporation of GNS was also confirmed by the increase in storage modulus and microhardness. An improved of dimensional stability was also detected in the nanocomposites compared to the neat polymers. Finally, electrical properties showed a significant increase with the GNS content.

Since graphite derivatives turn polyolefins very brittle, the alternative to synthesize nanocomposites with copolymers can be a very interesting solution. The presence of graphite nanosheets in PP copolymers has the potential to broaden the applications of these polyolefins, which are normally insulators, transforming them into thermally and electrically conductive materials. *In situ* polymerization let to control the amount of comonomer which gives the possibility to obtain materials with a wide range of mechanical properties.

Acknowledgments

The authors would like to thank CNPq, CAPES, FAPERG, Department of the Navy Grant N62909-11-1-7069 issued by Office of Naval Research Global, PROYECTO FONDECYT: 1130446, MINECO (CYTED-311RT0417, MAT2013-47972-C2-1-P and MAT2010-19883) for financial support. We also thank Nacional de Grafite Ltda./Brazil for the Micrograf supply.

Appendix A. Supplementary data

Supplementary data related to this article can be found at http://dx.doi.org/10.1016/j.polymer.2015.03.069.

References

[1] Etmimi HM, Mallon PE, Sanderson RD. Polymer/graphite nanocomposites: effect of reducing the functional groups of graphite oxide on water barrier properties. Eur Polym J 2013;49:3460–70.
[2] Ranjbartoreh AR, Wang B, Shen X, Wang G. Advanced mechanical properties of graphene paper. J Appl Phys 2011;109(014306):1–6.
[3] Arza CR, Jannasch P, Maurer FHJ. Network formation of graphene oxide in poly (3-hydroxybutyrate) nanocomposites. Eur Polym J 2014;59:262–9.
[4] Thostenson ET, Li C, Chou TH. Nanocomposites in context. Compos Sci Technol 2005;65:491–516.
[5] Todd AD, Bielawski CW. Thermally reduced graphite oxide reinforced polyethylene composites: a mild synthetic approach. Polymer 2013;54:4427–30.
[6] Xu JZ, Li ZM, Hsiao BS. In: Mittal V, editor. Polymer-graphene nanocomposites. England: Cambridge: RCS-Publishing; 2012. p. 227–63.
[7] Fim FC, Guterres JM, Basso NRS, Galland GB. Polyethylene/Graphite nanocomposites obtained by *in situ* polymerization. J Polym Sci Part A Polym Chem 2010;48:692–8.
[8] Milani MA, Quijada R, Basso NRS, Graebin AP, Galland GB. Influence of the graphite type on the synthesis of polypropylene/graphene nanocomposites. J Polym Sci Part A Polym Chem 2012;50:3598–605.
[9] Milani MA, González D, Quijada R, Basso NRS, Cerrada ML, Azambuja DS, et al. Polypropylene/graphene nanosheet nanocomposites by *in situ* polymerization: synthesis, characterization and fundamental properties. Compos Sci Technol 2013;84:1–7.
[10] Majada JML, Palza H, Guevara JL, Quijada R, Martínez MC, Benavente R, et al. Metallocene copolymers of propene and 1-Hexene: the influence of the comonomer content and thermal history on the structure and mechanical properties. J Polym Sci Part B Polym Phys 2006;44:1253–67.
[11] Zhang MQ, Rong MZ, Ruan WH. In: Kocsis JK, Fakirov S, editors. Nano- and micromechanics of polymer blends and composites. Germany: Munich Hanser; 2009. p. 91–140.
[12] Causin V, Marega C, Marigo A, Ferrara G, Ferraro A. Morphological and structural characterization of polypropylene/conductive graphite nanocomposites. Eur Polym J 2006;42:3153–61.
[13] Planes E, Duchet J, Maazouz A, Gerard JF. Characterization of new formulations for the rotational molding based on ethylene–propylene copolymer/graphite nanocomposites. Polym Eng Sci 2008;48:723–31.
[14] You F, Wang D, Cao J, Li X, Dang ZM, Hu GH. *In situ* thermal reduction of graphene oxide in a styrene–ethylene/butylene–styrene triblock copolymer via melt blending. Polym Int 2014;63:93–9.
[15] Xiong Y, Xie Y, Zhang F, Ou E, Jiang Z, Ke L, et al. Reduced graphene oxide/hydroxylated styrene–butadiene–styrene tri-block copolymer electroconductive nanocomposites: preparation and properties. Mater Sci Eng B 2012;177:1163–9.
[16] Ye L, Ding P, Zhang M, Qu B. Synergistic effects of exfoliated LDH with some halogen-free flame retardants in LDPE/EVA/HFMH/LDH nanocomposites. J Appl Polym Sci 2008;107:3694–701.
[17] Potts JR, Dreyer DR, Bielawski CW, Ruoff RS. Graphene-based polymer nanocomposites. Polymer 2011;52:5–25.
[18] Fim FC, Basso NRS, Graebin AP, Azambuja DS, Galland GB. Thermal, electrical, and mechanical properties of polyethylene–graphene nanocomposites obtained by *in situ* polymerization. J Appl Polym Sci 2013;128:2630–7.
[19] Etmimi HM, Sanderson RD. New approach to the synthesis of exfoliated polymer/graphite nanocomposites by miniemulsion polymerization using functionalized graphene. Macromolecules 2011;44:8504–15.
[20] Alsharaeh EH, Faisal NH, Othman AA, Ahmed R. Evaluation of nanomechanical properties of (styrene–methyl methacrylate) copolymer composites containing graphene sheets. Ind Eng Chem Res 2013;52:17871–81.
[21] Zhang P, Jiang K, Ye C, Zhao Y. Facile synthesis of V-shaped copolymer brushes grafted onto the surface of graphene oxide via coupling reactions. Chem Commun 2011;47:9504–6.

[22] http://www.grafite.com/Micrograf_en.asp, access March 23, 2015.
[23] Cheng HN, Lee GH. Two-dimensional NMR studies of polypropylene tacticity. Polym Bull 1985;13:549–56.
[24] Milani MA. Síntese de nanocompósitos de polipropileno e copolímeros poli(-propileno-1-octeno) com nanolâminas de grafite através da polimerização *in situ*. Ph.D. Thesis. Porto Alegre, Brazil: UFRGS; December 2013.
[25] Krache R, Benavente R, López-Majada JM, Pereña JM, Cerrada ML, Pérez E. Competition between α, β and γ polymorphs in a β-Nucleated metallocenic isotactic polypropylene. Macromolecules 2007;40:6871–8.
[26] Arranz-Andrés J, Peña B, Benavente R, Pérez E, Cerrada ML. Influence of isotacticity and molecular weight on the properties of metallocenic isotactic polypropylene. J Eur Polym J 2007;43:2357–70.
[27] Lorenzo V, Pereña JM, Fatou JMG. Relationships between mechanical properties and microhardness of polyethylenes. Angew Makromol Chem 1989;172:25–35.
[28] Palza H, López-Majada JM, Quijada R, Benavente R, Pérez E, Cerrada ML. Metallocenic copolymers of isotactic propylene and 1-Octadecene: crystalline structure and mechanical behavior. Macromol Chem Phys 2005;206:1221–30.
[29] Linares A, Canalda JC, Cagiao ME, García-Gutiérrez MC, Nogales A, Martúín-Gullón I, et al. Broad-band electrical conductivity of high density polyethylene nanocomposites with carbon nanoadditives: multiwall carbon nanotubes and carbon nanofiber. Macromolecules 2008;41:7090–7.